Supplementary Information (SI) for Journal of Materials Chemistry A.
This journal is © The Royal Society of Chemistry 2025

Electronic Supplementary Information for

Prediction of High Photoconversion Efficiency and Photocatalytic Water Splitting in Vertically Stacked TMD Heterojunctions MX_2/WS_2 and $MX_2/MoSe_2$ (M=Cr, Mo, W; X=S, Se, Te)

Jiancheng Ma[a], Jiafei Pang[a], Jinni Yang[a], Wanying Xie[a], Xiaoyu Kuang*[a] and Aijie Mao*[b]

[a]*Institute of Atomic and Molecular Physics, Sichuan University, Chengdu, 610065, China*

[b]*College of Physics, Sichuan University, Chengdu 610065, China.*

**E-mails: scu_kuang@163.com; scu_mij@126.com*

Computational Methods The Gibbs free energies for the oxygen evolution reaction (OER) and hydrogen evolution reaction (HER) are calculated based on the model proposed by Nørskov et al.[1,2] The OER follows these sequential steps:

$$* + \mathrm{H_2O} \longrightarrow *\mathrm{OH} + \mathrm{H^+} + \mathrm{e^-} \tag{1}$$

$$*\mathrm{OH} \longrightarrow *\mathrm{O} + \mathrm{H^+} + \mathrm{e^-} \tag{2}$$

$$*\mathrm{O} + \mathrm{H_2O} \longrightarrow *\mathrm{OOH} + \mathrm{H^+} + \mathrm{e^-} \tag{3}$$

$$*\mathrm{OOH} \longrightarrow * + \mathrm{O_2} + \mathrm{H^+} + \mathrm{e^-} \tag{4}$$

where * represents the absorption site on the slab for intermediates. For each step, the Gibbs reaction free energy (ΔG) is calculated by

$$\Delta G = \Delta E + \Delta E_{\mathrm{ZPE}} - T\Delta S + \Delta G_U + \Delta G_{\mathrm{pH}} \tag{5}$$

where ΔE is the total energy difference between reactants and products of reactions, ΔE_{ZPE} is the zero point energy correction, ΔS is the vibrational entropy change at finite temperature T, ΔG_U=-eU incorporates the effect of the electrode potential, where e is elementary charge, U is the electrode potential (U=1.23), ΔG_{pH} is the correction of the H^+ free energy. The calculations are performed at pH = 0.

The HER proceeds through the following steps:

$$* + \mathrm{H^+} + \mathrm{e^-} \longrightarrow *\mathrm{H} \tag{6}$$

$$*\mathrm{H} + \mathrm{H^+} + \mathrm{e^-} \longrightarrow * + \mathrm{H_2} \tag{7}$$

The free energy is calculated by

$$\Delta G_{*\mathrm{H}} = \Delta E_{*\mathrm{H}} + \Delta E_{\mathrm{ZPE}} - T\Delta S \tag{8}$$

$$\Delta E_{*\mathrm{H}} = E_{*\mathrm{H}} - E_* - \frac{1}{2}E_{\mathrm{H_2}} \tag{9}$$

where ΔE_{*H} is the hydrogen chemisorption energy , where E_{*H}, E_* and E_{H_2} are the energies of absorbed slab, pure slab and H_2 gas, respectively.

The relaxation time (τ) and carrier mobility (μ) at 300 K have mathematical formulas that follow the deformation potential (DP) theory:[3–5]

$$\mu = \frac{e\hbar^3 C_{2D}}{K_B T m^* m_d {E_l}^2} \tag{10}$$

$$m^* = \hbar^2 \frac{\partial^2 E}{\partial^2 K} \tag{11}$$

$$\tau = \frac{\mu m^*}{e} \tag{12}$$

where K_B is the Boltzmann constant, T is the temperature (300 K), m^* is the effective mass, $m_d = \sqrt{m^* m_\perp^*}$ represents the average effective mass, $E_l = \Delta V/(\Delta l/l_0)$is the deformation potential constant (ΔV is the amount of change in the position of band edges caused by stresses), e is the electronic charge, $\hbar$ is the reduced Planck constant, $C_{2D} = [\partial^2 E_T/\partial(\Delta l/l)^2]/S_0$ is the modulus of elasticity (E_T is the total energy, and S_0 indicates the area of the optimized cell), K is the wave vector, E is the energy corresponding to the wave vector, and the τ is relaxation time. The light absorption coefficient of the heterogeneous structure can be obtained using the following formula:[6]

$$\alpha(\omega) = \sqrt{2}\omega[\sqrt{\varepsilon_1^2(\omega) + \varepsilon_2^2(\omega)} - \varepsilon_1(\omega)]^{1/2} \tag{13}$$

The real and imaginary parts of the complex dielectric function are represented as $\varepsilon_1(\omega)$and $\varepsilon_2(\omega)$, respectively.

The imaginary component of the dielectric matrix is calculated as a summation over the unoccupied states:

$$\begin{aligned} \varepsilon_2(\omega) = & \frac{4\pi^2 e^2}{\Omega} \lim_{q\to\infty} \frac{1}{q^2} \Sigma 2 w_k \delta(\varepsilon_{ck} - \varepsilon_{vk} - \omega) \\ & \times \langle \mu_{ck} + e_\alpha | \mu_{vk} \rangle \left\langle \mu_{ck+e_\beta} | \mu_{vk}^* \right\rangle \end{aligned} \tag{14}$$

where Ω represents the volume of unit cell, c and v refer to the conduction and valence band states, and μ_{ck} is an eigenstate of the wave vector k. The symbols α and β specify the x and y directions.

The PCE is determined using Scharber's method, which is described as follows:[6,7]

$$\eta = \frac{V_{OC} J_{SC} \beta_{FF}}{P_{solar}} = \frac{0.65(E_g^d - \Delta E_C - 0.3) \int_{E_g^d}^{\infty} \frac{P(\hbar\omega)}{\hbar\omega} d(\hbar\omega)}{\int_0^{\infty} P(\hbar\omega) d(\hbar\omega)} \tag{15}$$

where V_{OC}, J_{SC}, β_{FF}, and P_{solar} stand for the maximum open-circuit voltage ($V_{OC} = E_g^d - \Delta E_C - 0.3$) heterojunction, the short-circuit current limit of 100% for external quantum efficiency (EQE), the bound filling factor (β_{FF}=0.65), and the AM1.5 solar flux (AM1.5 is the average yearly sun intensity at latitude 30° north), respectively.

Table S1 Elastic constants C_{ij} (in N/m) of the 2H-MX_2/WS_2 and MX_2/$MoSe_2$ (M=Cr, Mo, W. X=S, Se, Te) heterojunctions.

Heterojunction	C_{11}	C_{12}	C_{66}	$C_{11}C_{22}$-C_{12}^2
CrS_2/WS_2	273.64	59.29	107.17	71362.33
$CrSe_2$/WS_2	249.91	59.45	95.23	58921.97
MoS_2/WS_2	286.27	62.71	111.78	78017.47
$MoSe_2$/WS_2	264.21	54.62	104.80	66825.60
WSe_2/WS_2	278.24	51.80	113.22	74732.80
$CrSe_2$/$MoSe_2$	215.38	50.05	82.67	43885.57
$CrTe_2$/$MoSe_2$	573.24	-237.32	405.28	272285.61
MoS_2/$MoSe_2$	252.11	55.57	98.27	60468.97
$MoTe_2$/$MoSe_2$	200.97	41.72	79.62	38646.84
WSe_2/$MoSe_2$	239.84	45.73	97.06	55433.16
WTe_2/$MoSe_2$	211.01	36.24	87.38	43210.75

Table S2 The optimized lattice parameters (l_a), band gaps (E_g) based on HSE06, * represents results from other references.

Heterojunction	l_a ($\AA$)	l_a* ($\AA$)	E_g (eV)	E_g * (eV)
CrS_2	3.02	3.00[8]	1.69	1.48[9]
$CrSe_2$	3.19	3.18[10]	0.70	0.69[11]
$CrTe_2$	3.49	3.49[10]	0.92	0.93[12]
MoS_2	3.16	3.16[13]	2.24	2.30[14]
$MoSe_2$	3.29	3.29[13]	2.02	2.07[14]
$MoTe_2$	3.52	3.52[13]	1.60	1.67[14]
WS_2	3.17	3.15[13]	2.38	2.44[14]
WSe_2	3.29	3.28[13]	2.12	2.20[14]
WTe_2	3.52	3.56[13]	1.61	1.67[14]

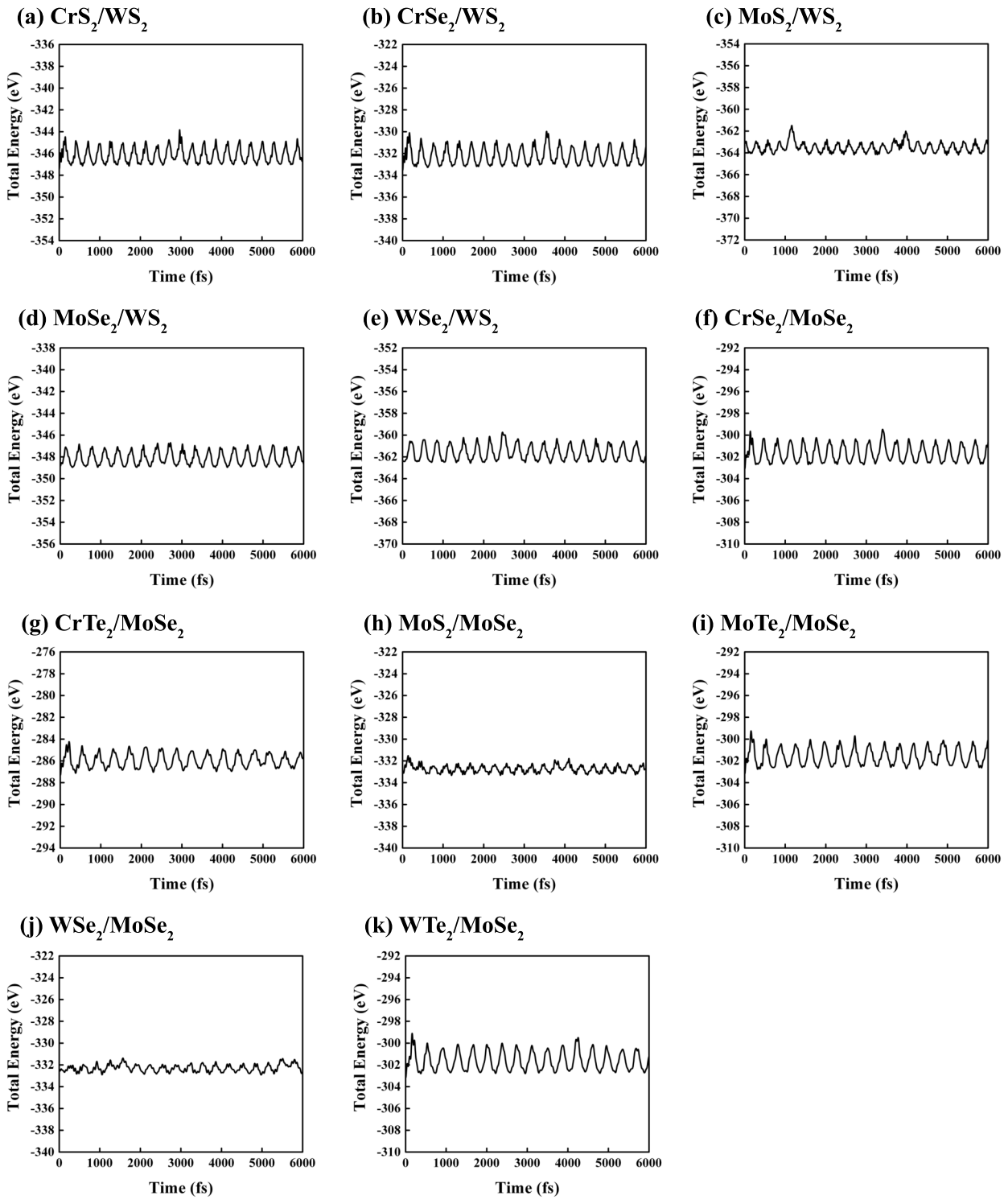

Fig. S1 (a)-(k) The time dependent evolution of the total energy in the AIMD simulation.

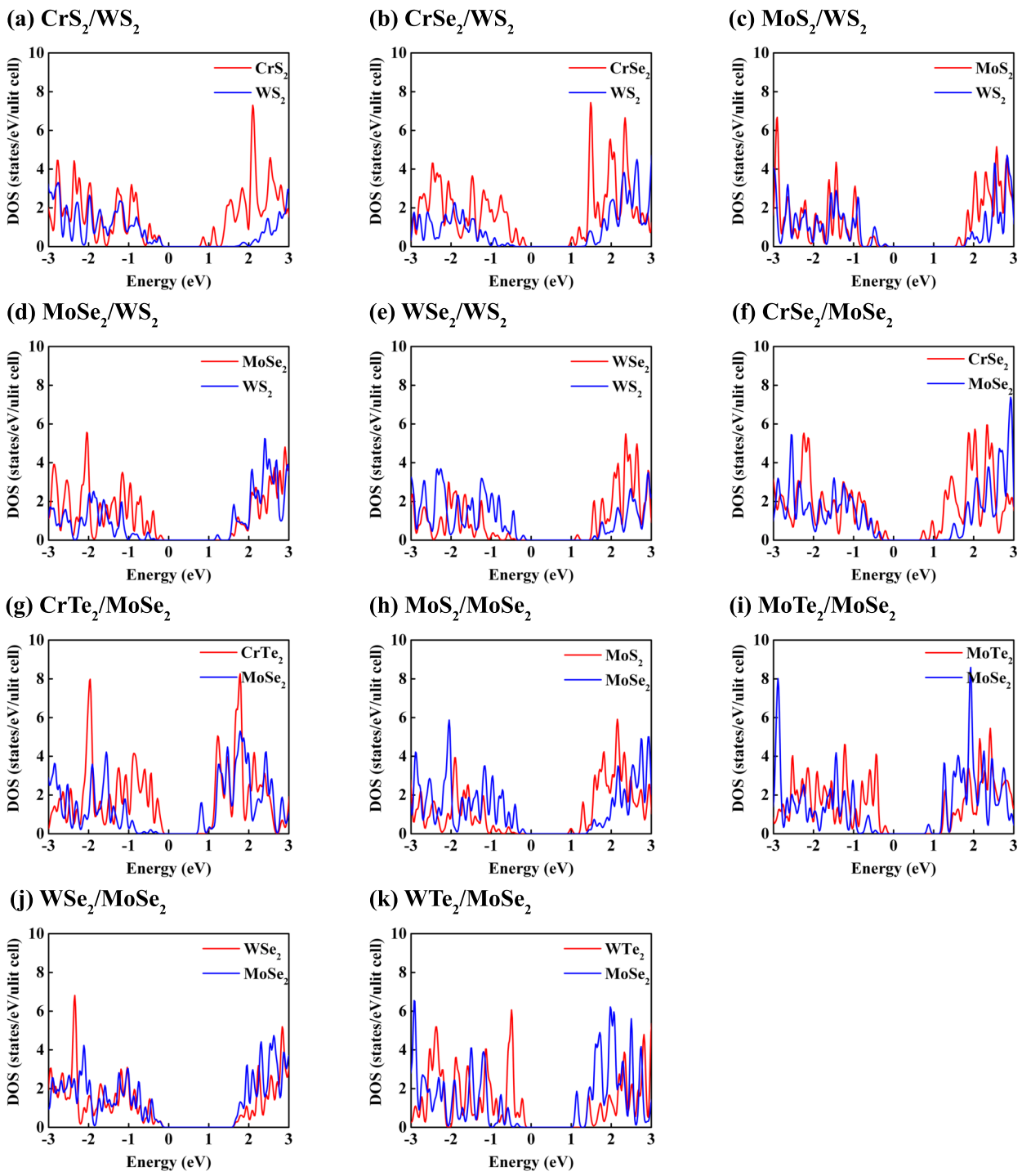

Fig. S2 The PDOS of 2H-MX_2/WS_2 and $MX_2/MoSe_2$ heterojunctions.

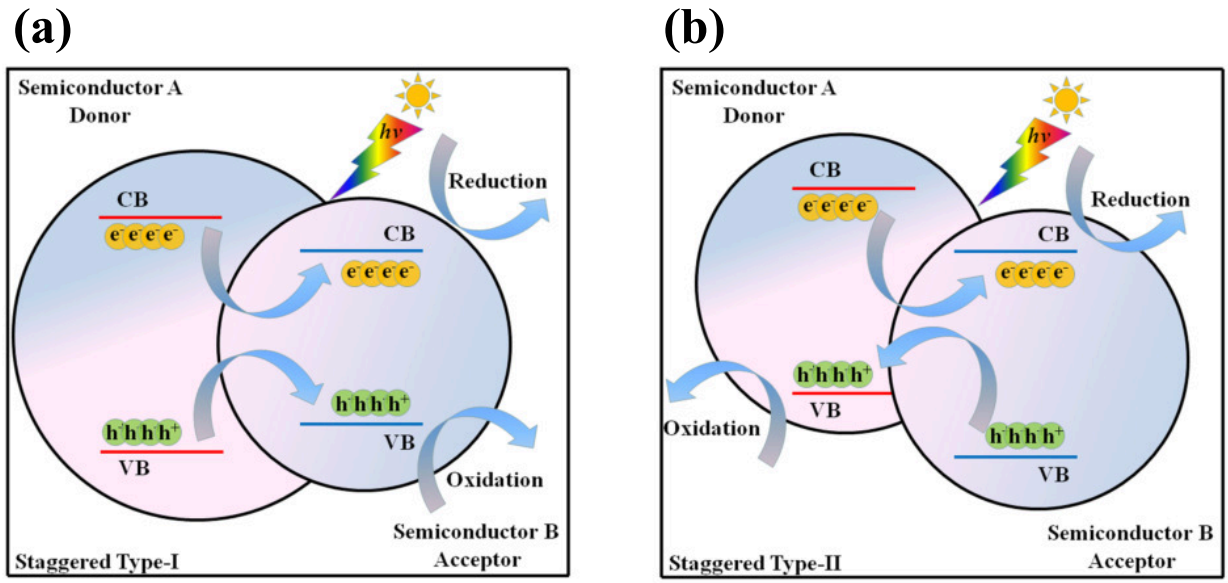

Fig. S3 Diagrammatic representation of the two distinct mechanisms for electron–hole pair separation in traditional light-responsive heterojunction photocatalysts: (a) type-I and (b) type-II.

Table S3 Calculated effective carrier mass m (m_0), deformation potential E (eV), in-plane stiffness C_{2D} (N/m), and carrier mobility μ ($cm^2\ V^{-1}\ s^{-1}$) along the *x* and *y* directions.

Carrier type	Heterojunction	m_x	m_y	E_x	E_y	C_x	C_y	μ_x	μ_y
Electron	MoS_2	0.412	0.415	8.27	2.94	137.7	136.9	69.34	543.21
	$MoSe_2$	0.566	0.419	7.49	2.61	113.7	114.4	50.84	570.58
	WS_2	0.114	0.556	7.25	2.16	109.3	143.2	258.87	783.25
	WSe_2	0.923	0.532	7.58	2.28	126.5	127.3	33.85	651.87
Hole	MoS_2	0.453	0.466	8.28	2.97	137.7	136.9	62.94	472.21
	$MoSe_2$	0.552	0.492	7.34	2.58	113.7	114.4	54.23	495.20
	WS_2	1.829	1.209	7.83	2.16	109.3	143.2	13.83	359.58
	WSe_2	0.448	0.437	7.50	2.18	126.5	127.3	71.24	868.68

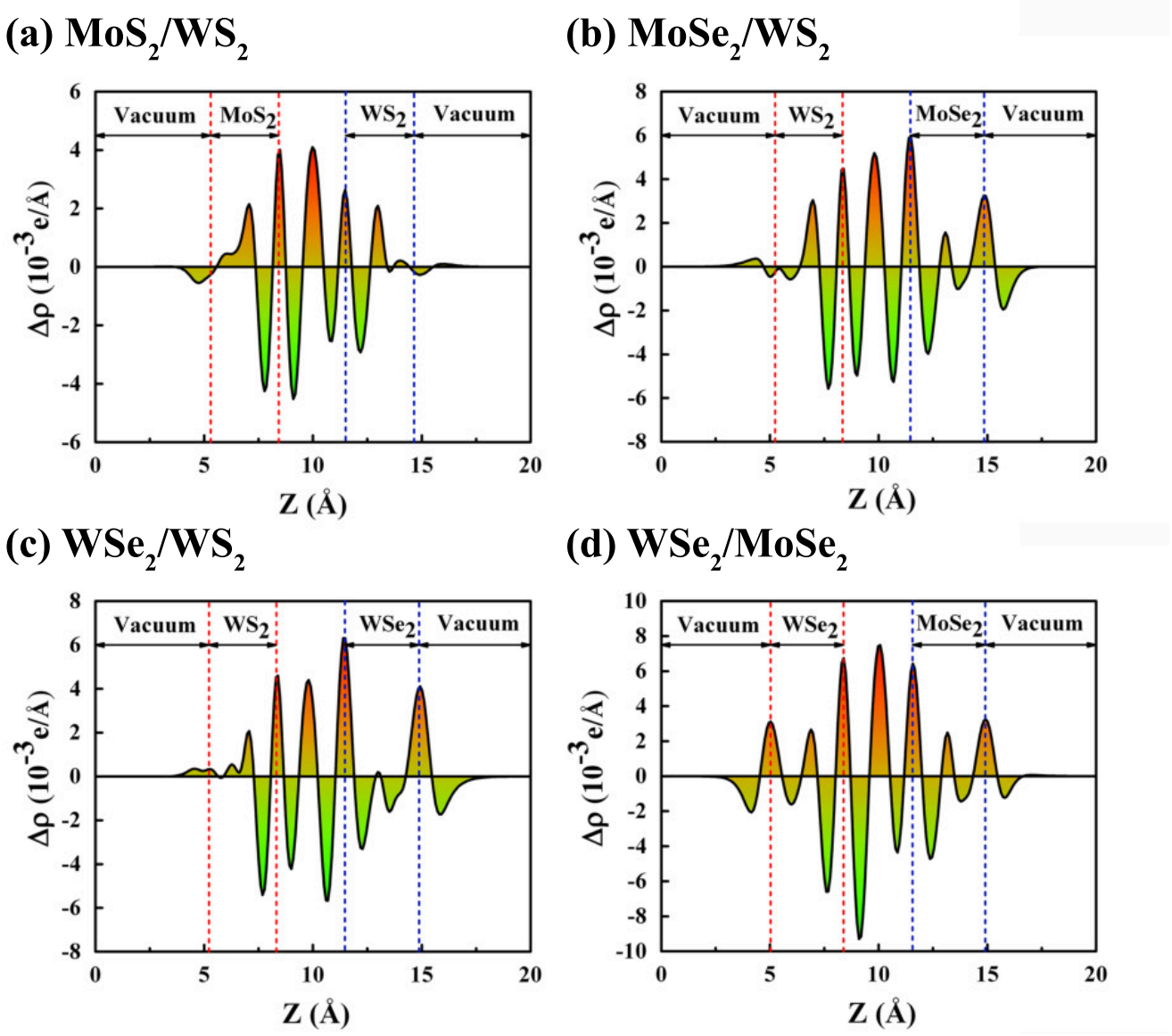

Fig. S4 (a)-(d) plane averaged potential drop along the z-direction of the MoS_2/WS_2, $MoSe_2/WS_2$, WSe_2/WS_2, and $WSe_2/MoSe_2$, respectively. Red represents charge accumulation, while green represents charge depletion.

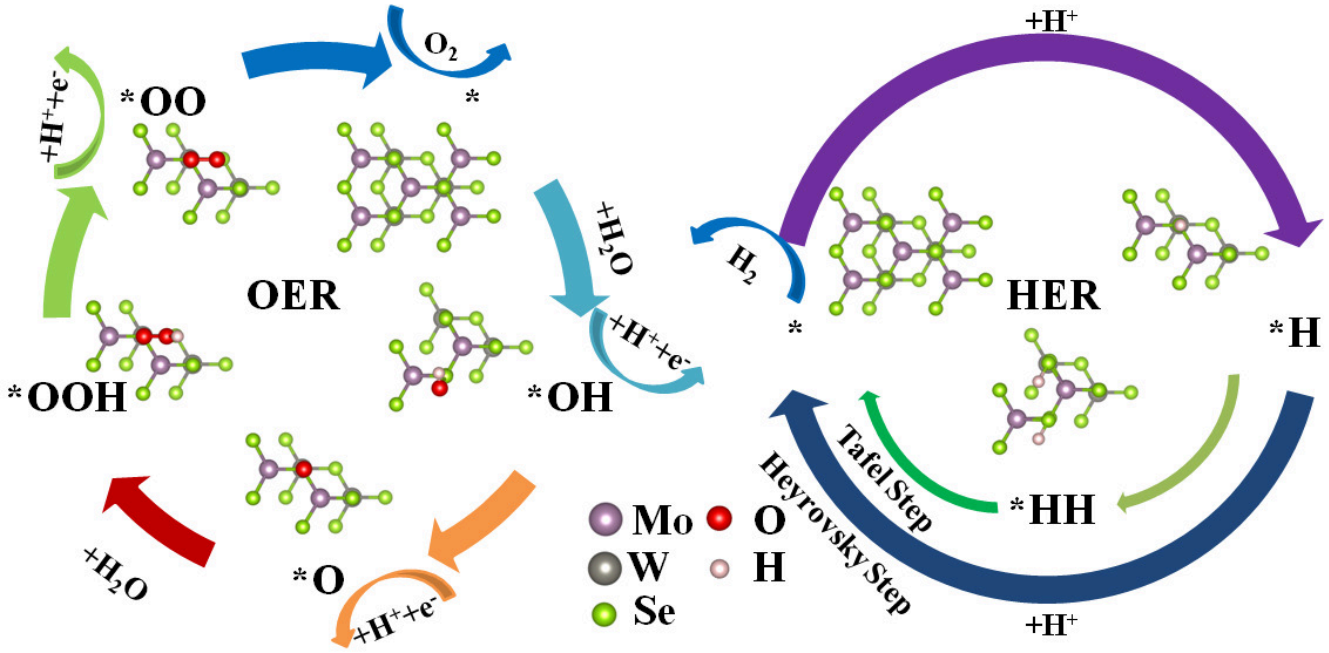

Fig. S5 The structural transitions of the entire OER and HER processes.

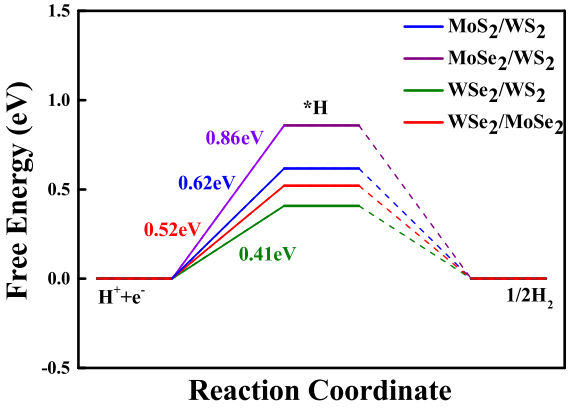

Fig. S6 Free energy diagram for the HER at the equilibrium potential (U=1.23V).

Table S4 The PCE of various heterojunctions. * represents this work.

Heterojunction	PCE	Heterojunction	PCE
Te/WTe_2	22.50%[15]	$Te/MoTe_2$	20.10%[15]
MoS_2/BP	20.42%[16]	phosphorene/MoS_2	17.50%[17]
$PtS_2/MoTe_2$	13.60%[18]	BP/SnSe	17.24%[19]
PN/WSe_2	13.80%[20]	MoS_2/ ψ-phosphorene	20.26%[21]
WS_2/MoS_2	12.93%[22]	WS_2/MoS_2*	13.82%
$MoSe_2/MoS_2$	18.64%[22]	$MoSe_2/MoS_2$*	15.83%
$MoSe_2/WS_2$	17.79%[22]	$MoSe_2/WS_2$ *	20.11%
$WSe_2/MoSe_2$	16.15%[22]	$WSe_2/MoSe_2$*	18.19%
WSe_2/WS_2	19.25%[22]	WSe_2/WS_2*	16.89%
WSe_2/MoS_2	14.35%[22]	CrS_2/WS_2*	9.00%
$WTe_2/MoSe_2$*	23.10%	$MoTe_2/MoSe_2$*	25.84%

Table S5 Atomic lattices in VASP POSCAR format.

CrS_2/WS_2		
1.00000000000000		
3.1055505547419062	0.0000000000000000	0.0000000000000000
-1.5527752773709531	2.6894860393690649	0.0000000000000000
0.0000000000000000	0.0000000000000000	21.2014999390000014
Cr S W		
1 4 1		
Direct		
0.6666660824732915	0.3333339465271052	0.3245239978819399
0.6666683901520472	0.3333316388475609	0.5407267840104879
0.6666684068844049	0.3333316221152032	0.6912896284138128
0.3333327251618314	0.6666673038383308	0.2561927154864136
0.3333327519017644	0.6666672770983908	0.3927263723128362
0.0000017254266638	0.9999982745734073	0.6159404738945256
$CrSe_2/WS_2$		
1.00000000000000		
3.1755542925400984	0.0000000000000000	0.0000000000000000
-1.5877771462700492	2.7501078439451416	0.0000000000000000
0.0000000000000000	0.0000000000000000	21.2014999390000014
Cr S Se W		
1 2 2 1		
Direct		
0.6666661614290703	0.3333338672792081	0.3214882731749569
0.6666682816649399	0.3333317472528634	0.5450217813300640
0.6666683091076067	0.3333317198081005	0.6930731698754116
0.3333328624135490	0.6666671667259862	0.2471302969788240
0.3333329269515133	0.6666671021867288	0.3957257403055010
0.0000015404333098	0.9999984597471112	0.6189607103352444

$CrTe_2/WS_2$		
1.00000000000000		
3.2886901931097521	0.0000000000000000	0.0000000000000000
-1.6443450965548760	2.8480909173629838	0.0000000000000000
0.0000000000000000	0.0000000000000000	21.2014999390000014
Cr S Te W		
1 2 2 1		
Direct		
0.6666674393444083	0.3333339595692735	0.3154145834825357
0.6666670950861118	0.3333318269114045	0.5529307384278184
0.6666669669859999	0.3333314416308184	0.6972911470370775
0.3333357069055367	0.6666669578594977	0.2322337069817664
0.3333325777987852	0.6666677189479771	0.3984999315265227
0.0000002958791683	0.9999981580810271	0.6250298645442882
MoS_2/WSe_2		
1.00000000000000		
3.1660921421639152	0.0000000000000000	0.0000000000000000
-1.5830460710819576	2.7419162258309129	0.0000000000000000
0.0000000000000000	0.0000000000000000	21.2014999390000014
Mo S W		
1 4 1		
Direct		
0.6666666870000029	0.3333333429999996	0.3237405409313610
0.6666666870000029	0.3333333429999996	0.5426076140989338
0.6666666870000029	0.3333333429999996	0.6909890797682081
0.3333333429999996	0.6666666870000029	0.2498336015311793
0.3333333429999996	0.6666666870000029	0.3975112134683414
0.0000000000000000	0.0000000000000000	0.6167179822019762

$MoSe_2/WS_2$		
1.00000000000000		
3.2262119268888956	0.0000000000000000	0.0000000000000000
-1.6131059634444478	2.7939814866724508	0.0000000000000000
0.0000000000000000	0.0000000000000000	21.2014999390000014
W Se Mo S		
1 2 1 2		
Direct		
0.6666666870000029	0.3333333429999996	0.3200840484661143
0.6666666870000029	0.3333333429999996	0.5403913972699925
0.6666666870000029	0.3333333429999996	0.7005349871969599
0.0000000000000000	0.0000000000000000	0.6203710258167519
0.3333333429999996	0.6666666870000029	0.2468445656053433
0.3333333429999996	0.6666666870000029	0.3931740076448307
$MoTe_2/WS_2$		
1.00000000000000		
3.3261171299554873	0.0000000000000000	0.0000000000000000
-1.6630585649777436	2.8796123074976441	0.0000000000000000
0.0000000000000000	0.0000000000000000	21.2014999390000014
Mo S Te W		
1 2 2 1		
Direct		
0.6666874869365174	0.3333738200875587	0.3142950355090477
0.6666630706861199	0.3333239294945471	0.5546310497818041
0.6666630537439886	0.3333238875762206	0.6978144124231775
0.3333231457527219	0.6666450509674959	0.2251311347470732
0.3333220998838371	0.6666431439605986	0.4033976701210662
0.0000112249968041	0.0000202309135773	0.6261306694178330

WSe_2/WS_2		
1.00000000000000		
3.2260240174904533	0.0000000000000000	0.0000000000000000
-1.6130120087452267	2.7938187523597935	0.0000000000000000
0.0000000000000000	0.0000000000000000	21.2014999390000014
W Se S		
2 2 2		
Direct		
0.6666666870000029	0.3333333429999996	0.3193673122038163
0.0000000000000000	0.0000000000000000	0.6211002569801707
0.6666666870000029	0.3333333429999996	0.5406522070482893
0.6666666870000029	0.3333333429999996	0.7017011957291928
0.3333333429999996	0.6666666870000029	0.2461255895291430
0.3333333429999996	0.6666666870000029	0.3924534705093947
WTe2/WS2		
1.00000000000000		
3.3274440761286970	0.0000000000000000	0.0000000000000000
-1.6637220380643485	2.8816772715970096	0.0000000000000000
0.0000000000000000	0.0000000000000000	21.2014999390000014
W S Te		
2 2 2		
Direct		
0.6666660296117755	0.3333339994266069	0.3143855495921670
0.0000006058180233	0.9999993941460730	0.6260353055576928
0.6666679024033542	0.3333321266219968	0.5545650232159502
0.6666676005487133	0.3333324284722892	0.6976930474151857
0.3333339822083943	0.6666660467768892	0.2246998029917791
0.3333339614097355	0.6666660675561431	0.4040212432272341

$CrS_2/MoSe_2$		
1.00000000000000		
3.1690270144846413	0.0000000000000000	0.0000000000000000
-1.5845135072423207	2.7444609017830230	0.0000000000000000
0.0000000000000000	0.0000000000000000	21.2014999390000014
Cr Se S Mo		
1 2 2 1		
Direct		
0.6666659289284596	0.3333331668321691	0.3212315655591738
0.6666683577842321	0.3333323500066072	0.5380949431286481
0.6666683989000575	0.3333323282884706	0.7004988438134490
0.3333333300851891	0.6666670244755650	0.2536741598200365
0.3333334421716643	0.6666669952211990	0.3886702047353765
0.0000006241303865	0.9999981981759944	0.6192302549433180
$CrSe_2/MoSe_2$		
1.00000000000000		
3.2443991322063912	0.0000000000000000	0.0000000000000000
-1.6221995661031956	2.8097277339265974	0.0000000000000000
0.0000000000000000	0.0000000000000000	21.2014999390000014
Cr Se Mo		
1 4 1		
Direct		
0.6666672308518997	0.3333327972993061	0.3172708064279135
0.6666682767373615	0.3333317522376902	0.5434773047081407
0.6666682941711315	0.3333317348060731	0.7030301957025031
0.3333323216183715	0.6666677078125645	0.2438676437889384
0.3333324762456016	0.6666675531851283	0.3905755202042371
0.0000014823756302	0.9999985176592361	0.6231785011682618

$CrTe_2/MoSe_2$		
1.00000000000000		
3.4506760212821064	0.0000000000000000	0.0000000000000000
-1.7253380106410532	2.9883757959317561	0.0000000000000000
0.0000000000000000	0.0000000000000000	21.2014999390000014
Cr Se Te Mo		
1 2 2 1		
Direct		
0.6666665806848826	0.3333334483118620	0.3130727039500130
0.6666683600981784	0.3333316689034405	0.5510872939307134
0.6666683846819055	0.3333316443192516	0.7039114390049335
0.3333328047848383	0.6666672242180098	0.2295140129396174
0.3333328648814557	0.6666671641220887	0.3963890219333095
0.0000010868687355	0.9999989131253386	0.6274255002414364
$MoS_2/MoSe_2$		
1.00000000000000		
3.2258146521245914	0.0000000000000000	0.0000000000000000
-1.6129073260622957	2.7936413089919410	0.0000000000000000
0.0000000000000000	0.0000000000000000	21.2014999390000014
Mo S Se		
2 2 2		
Direct		
0.6666560500327350	0.3333439400399953	0.3199669524272792
0.0000116690442624	0.9999883417538271	0.6204738561101593
0.3333233589534004	0.6666766895177076	0.2470264494229326
0.3333238629638728	0.6666761854758576	0.3928083059719967
0.6666774961086617	0.3333225274829346	0.5404727937065346
0.6666776448970637	0.3333223787296831	0.7006516743611044

$MoTe_2/MoSe_2$		
1.00000000000000		
3.4022047713032970	0.0000000000000000	0.0000000000000000
-1.7011023856516485	2.9463957608187537	0.0000000000000000
0.0000000000000000	0.0000000000000000	21.2014999390000014
Mo Se Te		
2 2 2		
Direct		
0.6666666870000029	0.3333333429999996	0.3102414077960418
0.0000000000000000	0.0000000000000000	0.6301950438871629
0.6666666870000029	0.3333333429999996	0.5531552621862019
0.6666666870000029	0.3333333429999996	0.7073906219611175
0.3333333429999996	0.6666666870000029	0.2226379088017651
0.3333333429999996	0.6666666870000029	0.3977797873677105
$WSe_2/MoSe_2$		
1.00000000000000		
3.2909805621213541	0.0000000000000000	0.0000000000000000
-1.6454902810606771	2.8500727701518880	0.0000000000000000
0.0000000000000000	0.0000000000000000	21.2014999390000014
W Se Mo		
1 4 1		
Direct		
0.6666666870000029	0.3333333429999996	0.3163634203021957
0.6666666870000029	0.3333333429999996	0.5452536869047293
0.6666666870000029	0.3333333429999996	0.7030909912299705
0.3333333429999996	0.6666666870000029	0.2369904284290882
0.3333333429999996	0.6666666870000029	0.3956230524998503
0.0000000000000000	0.0000000000000000	0.6240784526341727

$WTe_2/MoSe_2$		
1.00000000000000		
3.4030712785983637	0.0000000000000000	0.0000000000000000
-1.7015356392991818	2.9471442251541613	0.0000000000000000
0.0000000000000000	0.0000000000000000	21.2014999390000014
W Se Te Mo		
1 2 2 1		
Direct		
0.6666668537847187	0.3333331644629638	0.3106092899926765
0.6666676415940316	0.3333323881881327	0.5527969467854419
0.6666676504078382	0.3333323793866754	0.7070238888062832
0.3333339024427104	0.6666661319064104	0.2225110428891099
0.3333339189525617	0.6666661154306937	0.3986307888276244
0.0000001148181354	0.9999998836251223	0.6298280146988660

References

1 J. K. Nørskov, J. Rossmeisl, A. Logadottir, L. Lindqvist, J. R. Kitchin, T. Bligaard and H. Jonsson, *The Journal of Physical Chemistry B*, 2004, **108**, 17886–17892.

2 J. K. Nørskov, T. Bligaard, A. Logadottir, J. Kitchin, J. G. Chen, S. Pandelov and U. Stimming, *Journal of The Electrochemical Society*, 2005, **152**, J23.

3 S.-i. Takagi, A. Toriumi, M. Iwase and H. Tango, *IEEE Transactions on Electron Devices*, 1994, **41**, 2357–2362.

4 J. Xi, M. Long, L. Tang, D. Wang and Z. Shuai, *Nanoscale*, 2012, **4**, 4348–4369.

5 J. Chen, J. Xi, D. Wang and Z. Shuai, *The journal of physical chemistry letters*, 2013, **4**, 1443–1448.

6 S. Saha, T. Sinha and A. Mookerjee, *Physical Review B*, 2000, **62**, 8828.

7 M. C. Scharber, D. Mühlbacher, M. Koppe, P. Denk, C. Waldauf, A. J. Heeger and C. J. Brabec, *Advanced materials*, 2006, **18**, 789–794.

8 M. R. Habib, S. Wang, W. Wang, H. Xiao, S. M. Obaidulla, A. Gayen, Y. Khan, H. Chen and M. Xu, *Nanoscale*, 2019, **11**, 20123–20132.

9 H. L. Zhuang, M. D. Johannes, M. N. Blonsky and R. G. Hennig, *Applied Physics Letters*, 2014, **104**, year.

10 C. M. Bastos, R. Besse, J. L. Da Silva and G. M. Sipahi, *Physical Review Materials*, 2019, **3**, 044002.

11 S. Tang, D. Wan, S. Bai, S. Fu, X. Wang, X. Li and J. Zhang, *Physical Chemistry Chemical Physics*, 2023, **25**, 22401–22414.

12 S. Bai, S. Tang, M. Wu, D. Luo, J. Zhang, D. Wan and X. Li, *Journal of Alloys and Compounds*, 2023, **930**, 167485.

13 M. Ge, L. Chu, F. Zeng, Z. Cao and J. Zhang, *Physical Chemistry Chemical Physics*, 2024, **26**, 23784–23791.

14 A. Dias, H. Braganca, J. P. A. de Mendonca and J. L. Da Silva, *ACS Applied Energy Materials*, 2021, **4**, 3265–3278.

15 K. Wu, H. Ma, Y. Gao, W. Hu and J. Yang, *Journal of Materials Chemistry A*, 2019, **7**, 7430–7436.

16 M. K. Mohanta, A. Rawat, N. Jena, Dimple, R. Ahammed and A. De Sarkar, *ACS Applied Materials & Interfaces*, 2020, **12**, 3114–3126.

17 H. Guo, N. Lu, J. Dai, X. Wu and X. C. Zeng, *The Journal of Physical Chemistry C*, 2014, **118**, 14051–14059.

18 S. Yin, Q. Luo, D. Wei, G. Guo, X. Sun, Y. Tang and X. Dai, *Results in Physics*, 2022, **33**, 105172.

19 W. Dou, A. Huang, Y. Ji, X. Yang, Y. Xin, H. Shi, M. Wang, Z. Xiao, M. Zhou and P. K. Chu, *Physical Chemistry Chemical Physics*, 2020, **22**, 14787–14795.

20 X. Zheng, Y. Wei, K. Pang, N. Kaner Tolbert, D. Kong, X. Xu, J. Yang, X. Li and W. Li, *Scientific Reports*, 2020, **10**, 17213.

21 H. Wang, X. Li, Z. Liu and J. Yang, *Physical Chemistry Chemical Physics*, 2017, **19**, 2402–2408.

22 K. Dange, R. Yogi and A. Shukla, *arXiv preprint arXiv:2501.08138*, 2025.